VOL. 11, NO. 23, DECEMBER 2016 ISSN 1819-6608
ARPN Journal of Engineering and Applied Sciences

www.arpnjournals.com

THE EFFECT OF Gd_2O_3NANOPARTICLES ADDITION ON MICROSTRUCTURAL AND ELECTRICAL PROPERTIES OF YBCO SUPERCONDUCTOR

Aima Ramli[1, 2], S. A. Halim[1], S. K. Chen[1] and M. M. Awang Kechik[1]
[1]Superconductivity and Thin Films Laboratory, Department of Physics, Universiti Putra Malaysia, Serdang, Selangor, Malaysia
[2]Department of Physics, School of Fundamental Science, Universiti Malaysia Terengganu (UMT), Kuala Terengganu, Malaysia
E-Mail: aima.ramli@umt.edu.my

ABSTRACT

Polycrystalline samples of $YBa_2Cu_3O_{7-\delta}$ have been synthesized via co-precipitation method with the inclusion of Gd_2O_3 ($0 \leq x \leq 1.0$). The effect of Gd_2O_3 nanoparticles on the superconducting properties and crystal structure of $YBa_2Cu_3O_{7-\delta}$ were investigated. The superconducting transition temperature (T_c) of each sample was measured by a standard four point probe method. As the inclusion of nano-Gd_2O_3 increases, the T_c of samples decrease from 92 K for x = 0.0 to 80 K for x = 1.0 wt% attributable to oxygen vacancy disorder. The crystal lattice parameters of all samples were determined by X-ray diffraction (XRD) with the Rietveld refinement technique. It was found that the samples are predominantly single phase perovskite structure Y-123 with orthorhombic and secondary phase, Y-211 for samples x = 0.2 - 1.0 wt%. The microstructural properties of samples were observed by Scanning Electron Microscope (SEM). The structure becomes more porous than the pure sample and the grain size significantly decrease. The addition of nano-Gd_2O_3 disturbs the grain growth of YBCO (123), thus resulting in the degradation of superconducting properties of the samples. The effect of Gd_2O_3 addition for intergranular critical current density, J_c and the presence of weak links that coupled the superconducting grains were also defined in AC susceptibility measurement in the range 0.005 Oe to 3.0 Oe.

Keywords: YBCO, superconducting transition temperature, co-precipitation, AC susceptibility, critical current density.

1. INTRODUCTION

The discovery of high temperature superconductivity in the copper oxide based materials by J. G. Bednorz and K. A. Müller in 1986 resulted in worldwide interest in these materials. Intense research efforts into superconductivity were undertaken during the last two decades. Several important methods such as solid-state [1] and wet chemical methods have been used to synthesize YBCO. Wet chemical methods can be separated into co-precipitation [2], sol-gel process [3], spray drying [4] and pyrophoric process [5]. Many of the copper oxide based materials, such as $YBa_2Cu_3O_{7-\delta}$, were found to have a T_c higher than the boiling point of liquid nitrogen (~77 K). Recently, many researchers have focused on investing the superconducting properties of high temperature superconductor $YBa_2Cu_3O_{7-\delta}$ (YBCO) because this type of superconductor receives enormous attention due to their captivating properties, e. g. relatively high T_c, high J_c and excellent capabilities of trapping magnetic fields [6,7]. Previous studies showed that critical temperature, T_c is sensitive to impurities and doping elements which suppress the superconductivity and may locally modify the crystalline structure and generate defects such as twins, tweed, and inhomogeneous micro-defects, and can act as additional pinning centres [8,9]. In this work, we report the results of superconducting properties of $YBa_2Cu_3O_{7-\delta}$ with inclusion of small range Gd_2O_3, x = 0.0 – 1.0 wt%. The samples were prepared by using co-precipitation method. The results on crystal structure and phase formation analysis are reported as well.

2 MATERIALS AND METHODS

Powder of constituent metal acetates of Yttrium (III) acetate ($Y(CH_3COO)_3.4H_2O$), barium acetate ($Ba(CH_3COO)$) and copper (II) acetate ($Cu(CH_3COO)_2$) with purity > 99%, were weighed in their molar ratio 1:2:3 and dissolved in acetic acid, namely solution A. Meanwhile, solution B containing 0.5M oxalic acid was prepared in a mixture of deionized high-purity water: isopropanol (v/v = 1:1.5). Solution B was added drop-wise into solution A in an ice bath with continuous stirring in order to completely dissolve the solutions. A uniform, stable, blue suspension was formed and the slurry was filtered after 5-10 minute of reaction. After filtration, the filtrated cake was allowed to dry at 80 ºC overnight. The dried blue precipitates were ground prior to thermal treatment at 900 ºC in air for 15 h. The calcined powders was added with nano-Gd_2O_3 (x = 0 - 1.0 wt%) and reground in agate mortar until well-mixed. The mixed powders were pressed into pellets of 13 mm diameter using Specac manually operated hydraulic press. The pellets were sintered at 920 ºC for 15 h in air and cooled slowly to room temperature in furnace at a rate 1 ºC/min.

The thermal decomposition behaviour of the coprecipitated precursor powders were analysed by using a Mettler Toledo thermobalance (model TGA/SDTA 851^e) with a heating rate of 10 ^{o}C/min. Samples of approximately 8 g were placed in aluminium pans and heated from 30^{o}C to 900^{o}C under a dynamic flow of nitrogen at 50 mL/min. The structure and phase identification of the powder samples ground from sintered pellets were examined by powder XRD using a Philips 1710 diffractometer with Cu Kα radiation. Refinement of the X-ray diffraction data was carried out by the Rietveld

method. The electrical resistance measurements were made by using standard four-probe method, in a closed cycle helium cryostat at temperatures between 20 K and 300 K. The surface morphology of the samples was carried out by scanning electron micrograph (SEM). The AC susceptibility measurement was performed using a Cryogenic Balanced Inductive Detector (CryoBIND) SR830 lock-in-amplifier at a frequency 123 Hz to study the flux penetration when samples were heated from 75 K to 95 K with the driving ranging from 0.005 Oe to 3.0 Oe.

3 RESULTS AND DISCUSSIONS

3.1 Thermo gravimetric analysis (TG / DTG)

Figure-1 indicates the thermal decomposition of the YBCO precursor powder during the TG measurement and DTG (derivative of the weight loss curve). From this method, the proper sintering temperature could be estimated. As shown in drop 1 and 2 (< 240 ^{o}C), approximately 19% weight loss is attributed to the dehydration of moisture and water in lattice of the oxalate salts. This dehydration process is also proved by DTG measurements where the drop peaks are in the same temperature range and could be clearly seen. A sharp drop peak is observed in drop 3, approximately 18% weight loss in the temperature range of 250^{o}C to 356^{o}C as the decomposition of the yttrium oxalate salts to the corresponding carbonates and copper oxalate to corresponding copper oxide. The XRD spectrum of the samples is shown in Figure-2. It is noteworthy to remark that rare earth carbonates are amorphous and they are so difficult to be detected by XRD analysis [10].

In drop 4, the decomposition of barium oxalate corresponding barium carbonate is observed in the range of temperature 365.7^{o}C - 568.8^{o}C respectively. On heating to higher temperature, the composition of barium carbonate to barium oxide takes place at near 760^{o}C and fully decomposed at 896^{o}C. At temperature near 900^{o}C, the formation of YBCO 123 (Y123) phase was produced. However, at temperature above 950^{o}C, the superconducting YBCO phase is damaged due to oxygen loss and melting [11]. Consequently, from the TG plots, the total losses of mass during the entire thermal decomposition process were found to be 55%.

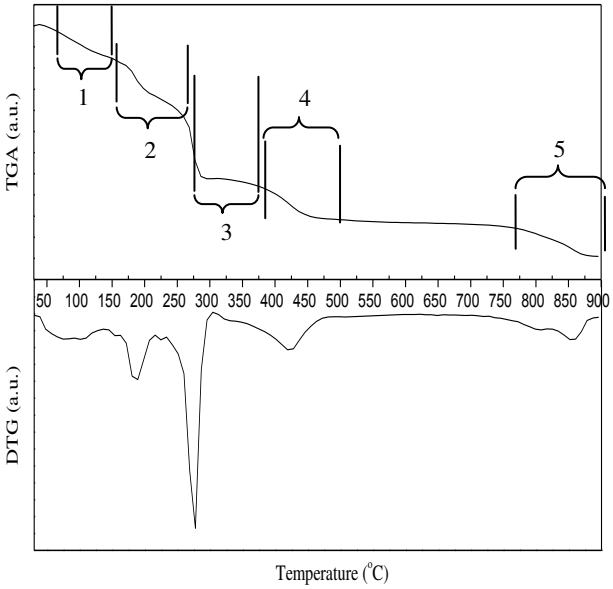

Figure-1. Thermogravimetric (TG/DTG) analysis of the YBCO oxalate powder.

3.2 X-ray Diffraction (XRD) pattern

Figure-2 shows the refined θ-2θ diffraction pattern of YBCO added with various amount of Gd_2O_3. Those data was compared with that of ICDD-PDF-2 database to verify the structural parameters. It showed that the pure sample is dominantly single phase and consist of perovskite-like structure Y123 corresponding to orthorhombic *Pmmm* symmetry. The lattice parameters and unit cell volume for pure YBCO sample obtained from the data are a = 3.8211 Å, b =3.8881 Å, c = 11.690 Å and V = 173.68 Å. The highest intensity diffraction patterns mainly show Y123 (013) and (103) peaks at approximately 32.60^{o} and 32.90^{o} (2-theta).The structural parameters for the samples were refined so that the calculated pattern fits the observed spectrum very well. It has been noticed that some small intensity peaks of secondary phases, Y-211 and impurity Gd_2O_3 are finely distributed in samples x = 0.2 – 1.0 wt% with peak approximately at 30^{o} and 29^{o}. The volume fraction of non-superconducting phase, Y211 increases from 12.2% to 28.7% as the addition of Gd_2O_3 increase. This condition might affect the superconducting properties in this system.

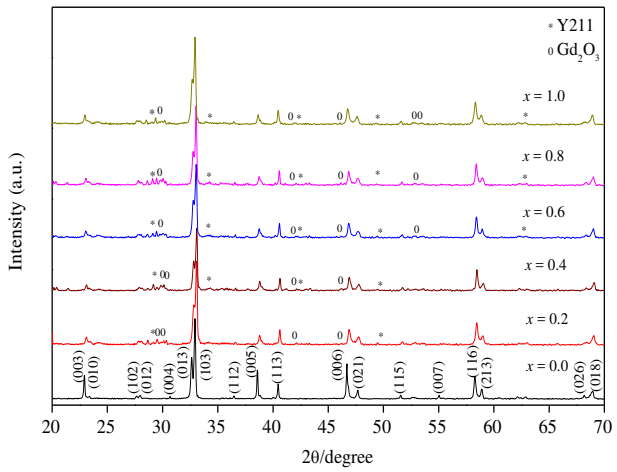

Figure-2. X-ray diffraction pattern of YBCO with various addition of Gd_2O_3.

The lattice parameters along *a*-, *b*-, and *c*- axis versus Gd_2O_3 weight percent; *x* is plotted in Figure-3. The lattice constant, *a* increase in samples *x* = 0.2 - 0.6 wt% and slightly decrease in *x* = 0.8 wt% and 1.0 wt%. On the other hand, lattice constants *b* and *c* decrease as the concentration of Gd_2O_3 increase. While the unit cell volume values, *V* increased in $x \leq 0.4$ wt% and slightly decreased in 0.6 - 1.0 wt% as shown in Table-1.

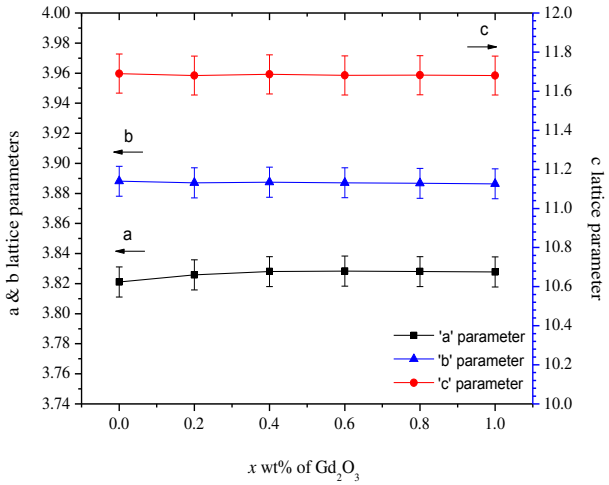

Figure-3. Variation of lattice constants along *a*-, *b*- and *c*-axis for YBCO added with various amounts of Gd_2O_3.

Table-1. Refined unit cell lattice parameters, *a*, *b* and *c* axes for YBCO added with various amounts of Gd_2O_3.

x, Gd_2O_3	*a* (Å)	*b* (Å)	*c* (Å)	V (Å^3)
0.0	3.8211	3.8881	11.690	173.6762
0.2	3.8258	3.8870	11.680	173.6919
0.4	3.8280	3.8875	11.686	173.9034
0.6	3.8283	3.8871	11.681	173.8248
0.8	3.8280	3.8867	11.682	173.8082
1.0	3.8278	3.8864	11.680	173.7559

All samples with Gd_2O_3 addition are maintained with orthorhombic structure comparable to the pristine sample which is calculated from the equation:

$$Orthorhombicity = \left|\frac{(b-a)}{(a+b)}\right|$$

as reported by Giri[12].Upon increasing the addition level of Gd_2O_3, it gives the difference between lattice constants *a* and *b*, thus reduces the orthorhombicity of the system linearly as shown in Figure-4. Refinements with two phases also tell us that Gd_2O_3 and YBCO (123) coexist in the composites and the Gd_2O_3 grains have successfully been inserted among YBCO grain boundaries. The variation in lattice constants and unit cell volume may cause and induce the tensile strain in YBCO crystalline grain [13].

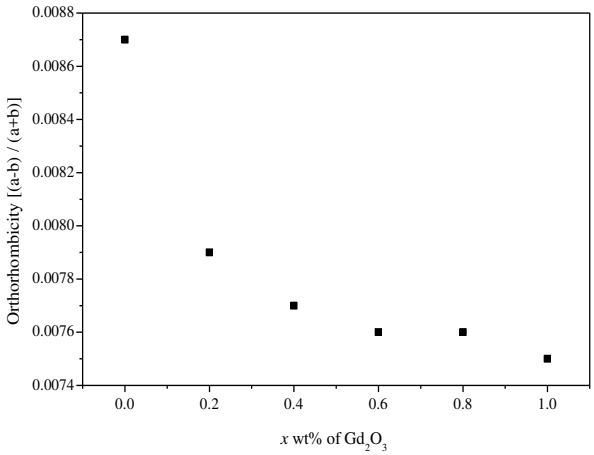

Figure-4. Calculated orthorhombicity versus YBCO added with various amounts of Gd_2O_3.

3.3 Electrical resistance

Figure-5 shows the dc conductivity of YBCO with various amounts of Gd_2O_3 was measured by four point probe method.It was found that the pure sample exhibits metallic behaviour in the normal state at $T_{c\text{-onset}}$ = 92 K and reaches the zero resistance at $T_{c\text{-offset}}$= 88 K. Samples with *x* = 0.2 - 1.0 wt% start to show semimetallic-semiconducting behaviour in the normal state and a superconducting transition to zero resistance. $T_{c\text{-onset}}$ is about 91, 90, 89, 88 and 80 K for samples *x* = 0.2, 0.4, 0.6, 0.8 and 1.0 wt%, respectively. The samples with additives show a two-step transition due to phase separation in YBCO at different doping level. The presence of a double superconducting transition can be attributed to the existence of another superconducting phase or impurities which can contribute from the chemical reaction of Gd_2O_3 with the matrix.The critical temperature (T_c) is also related to the oxygen deficiency, δ through the generic phase diagram of cuprate superconductors [14]. It was believed that oxygen content in this system was decreased and found that T_c follows an approximately parabolic dependence upon the doped holes concentration, *p*. In such

case T_c appears to be maximized around $p \approx 0.16$. The charge carrier (number of holes) concentration-critical temperature dependence can be defined by using the following relation [15]:

$$\frac{T_c}{T_{c-max}} = 1 - 82.6\,(p - 0.16^2)$$

The hole concentrations of the samples have been calculated and the results are shown in Table-2.

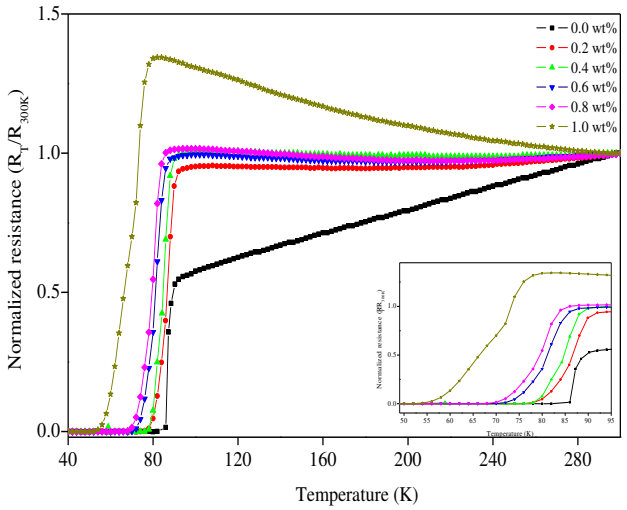

Figure-5. Normalized critical temperature, T_c for samples sintered with various amounts of Gd_2O_3.

Table-2. The $T_{c\text{-onset}}$, $T_{c\text{-offset}}$, transition width, ΔT_c and hole concentrations, p for YBCO added with various amounts of Gd_2O_3.

x,Gd_2O_3 (wt%)	$T_{c\text{-onset}}$(K)	$T_{c\text{-offset}}$(K)	ΔT_c(K)	Hole concentrations, p
0.0	92	88	4	0.160
0.2	91	80	9	0.149
0.4	90	78	12	0.144
0.6	89	74	15	0.140
0.8	88	72	16	0.137
1.0	80	58	22	0.120

3.4 Microstructure analysis SEM

Figure-6 display the SEM images of YBCO samples with addition of Gd_2O_3 at x = 0.2, 0.4, 0.6, 0.8 and 1.0 wt% taken at different magnifications. A very clear grain can be seen in samples x = 0.2, 0.8 and 1.0 wt%. However, in the case of samples x = 0.4 and 0.6 wt%, some agglomeration, rough and smeared on surface as shown in Figures 6 (a) and (b). The grains are not clearly seen indicating that the samples were not well polished. Luckily, the average size of 100 grains for these samples can still be measured using software Image J. It was observed that the grain size of the samples decreased as the addition of Gd_2O_3 increased. The grain size for each composition of x = 0.2 - 1.0 wt% is about 1.592 µm, 1.508 µm, 1.419 µm, 1.448 µm and 1.424 µm.

The pores and voids are obviously can be seen in every figure indicates that the samples are not closely packed, not good in grains connectivity and have lower density [16]. A molten-like structure was discovered in the highest additive of Gd_2O_3, x = 1.0 wt% which might be due to high temperature sintering. All these factors will contribute to the depression of superconductivity properties especially in the critical current density, J_c.

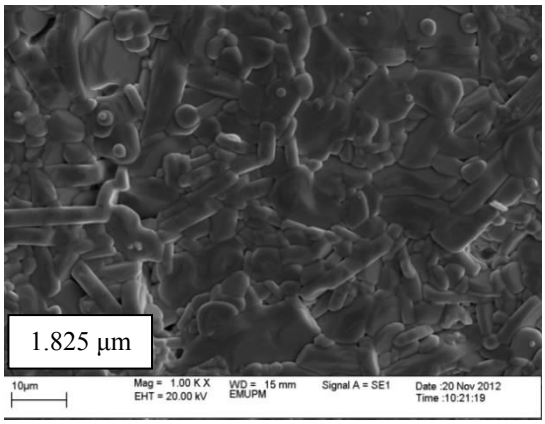

(a)

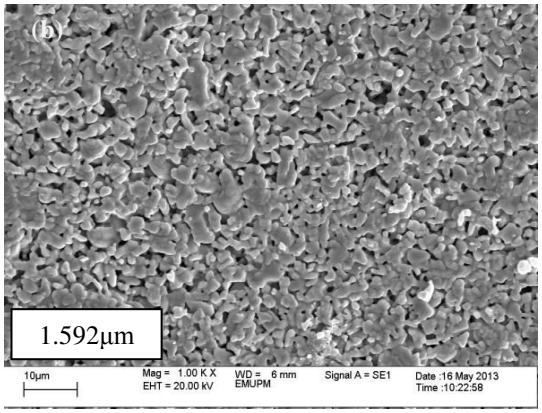

(b)

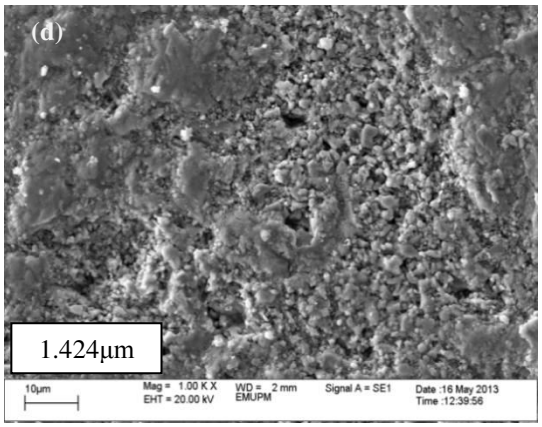

(c)

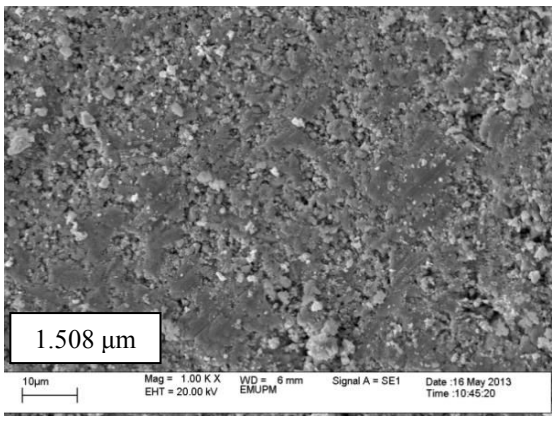

(d)

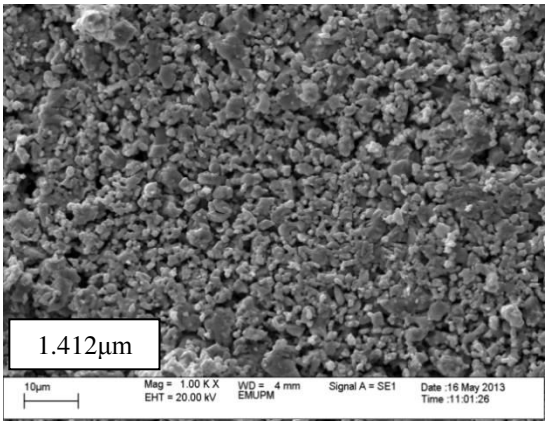

(e)

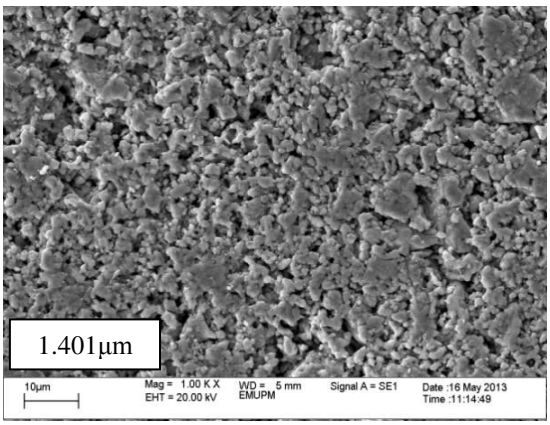

(f)

Figure-6.SEM images with average grain size measured from Image J for YBCO + Gd_2O_3; (a) 0.0 wt%, (b) 0.2 wt%, (c) 0.4 wt%, (d) 0.6 wt%, (e) 0.8 wt% and (f) .10 wt%.

3.5 AC Susceptibility analysis

Since superconductor polycrystalline samples are granular in nature, the best way to study their superconducting properties is by magnetization measurements rather than transport measurements. Ac susceptibility is considered as a non-destructive method, without electrical contacts and the sample size can be very small yet in the powder form [17]. Basically, the transition change from a normal state to the superconducting state is characterized by the resistivity loop. But in superconductor, the magnetic manifestation of zero resistivity is that a material is said to be superconductor if it shows perfect diamagnetic shielding (Meissner effect);where its susceptibility, χ value is absolutely -1. Thus, the critical temperature, T_c, where resistivity tends to zero can be determined from this an Ac susceptibility measurement. Sometimes the onset temperature of transition, $T_{c\text{-onset}}$, is used to describe the transition temperature and therefore it shows the quality of the sample. Onset temperature is observed from the first sign of zero resistance and defined as the onset upon cooling, even if the measurement is made upon warming. $T_{c\text{-onset}}$ is also often related to the Meissner shielding, resulting in decreasing of χ', while χ" may remain zero in ideal superconductor with no obvious loss.

Figure-7 show the temperature dependence of susceptibility losses of studied YBCO with addition of $x Gd_2O_3$ (x = 0.2, 0.4, 0.6, 0.8 and 1.0 wt%) samples under magnetic field amplitude 0.005 Oe to 3 Oe at a fixed frequency of 123 Hz. The experimental ac susceptibility data χ' (T) and χ" (T) were normalised to $|\chi|$ at the lowest temperature and the lowest ac field amplitude for each sample since the demagnetising correction would cause χ' = -1. In polycrystalline HTS, a typical characteristic of ACS is the appearance of two step diamagnetic transition in χ' and accompanied by double peaks of χ" due to the intra-granular and inter-granular transition. In the real part, χ' (T), samples with content 0.2 and 0.4 wt% of Gd_2O_3 show a double-step transition up to field of 0.1 Oe. However, as the field amplitude increase from 0.5 - 3 Oe, the curve showed single–step diamagnetic transition. Besides, samples with content 0.6 wt% and 0.8 wt% Gd_2O_3 the curves show single-step transition in the field amplitude $\geq$ 0.1 Oe. In the case of highest amount of Gd_2O_3, x = 1.0 wt %, the diamagnetic transition curves show single-step and remains unchanged at around 90.5 K in all fields amplitude. This is due to the effect of maximum Gd_2O_3 adding which weakens pinning force in the system and poor coupled in the grain.

The imaginary part, χ" (T) which represent the presence of hysteretic and flux motion losses [18] is the reflection from the real part, χ' (T), because relative alter of T_p with H_{ac}. Thus, T_p in inter-granular was observed at low field only in samples 0.2 wt % (T_p = 80, 79.9, 78.3 K at 0.005, 0.01 and 0.05 Oe) and 0.4 wt% (T_p = 78 and 77.5 K at 0.005 and 0.01 Oe), respectively. As the field increased, T_p shift to the lower temperature and peak becomes broaden. The amount of the shift as a function of the field amplitude, H_{ac} is directly proportional to the magnitude or strength of the pinning force. The weaker the pinning, the smaller the critical current [19]. This can be attributed to the some defects such as vacancies, twin boundaries, grain misorientation and strain in the sample even though the effect is small which are responsible for energy losses in χ" (T) peak [20].

However, it has been noticed that as the adding of Gd_2O_3 increased, the intra-granular peak is clearly able to be seen and height of peak slightly increases as shown in the inset of the graph in every figure but T_p in inter-

granular losses unseen because it is below minimum measurement range (a limitation of using liquid nitrogen). This peak (near T_c) is the manifestation of the field penetration into the grains or indication of hysteresis loss for the motion of intra-granular Abrikosov vortices inside the grains [21]. A broad separation between inter- and intra-granular loss peaks indicates that the grains were not well-coupled. Because of ac susceptibility measurement is temperature dependence, this measurement should be done in lower temperature (liquid helium) so that the inter-granular peak is visible and further investigation could be done.

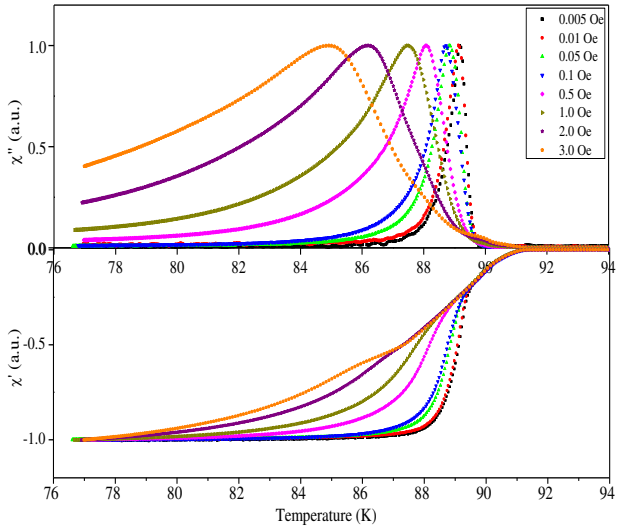

(a)

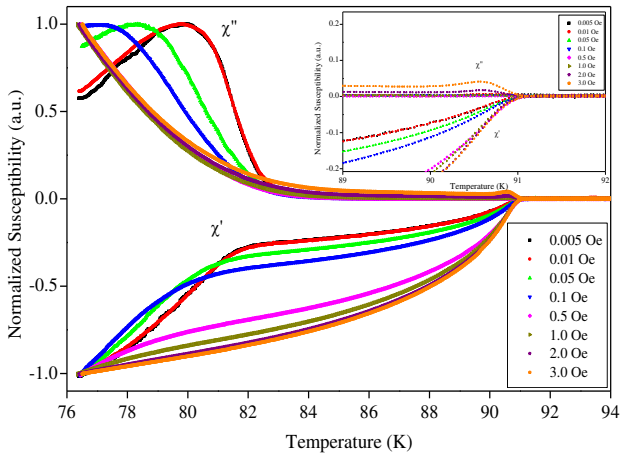

(b)

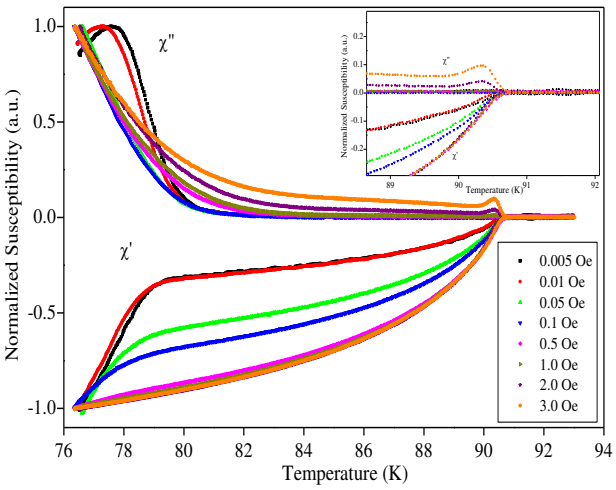

(c)

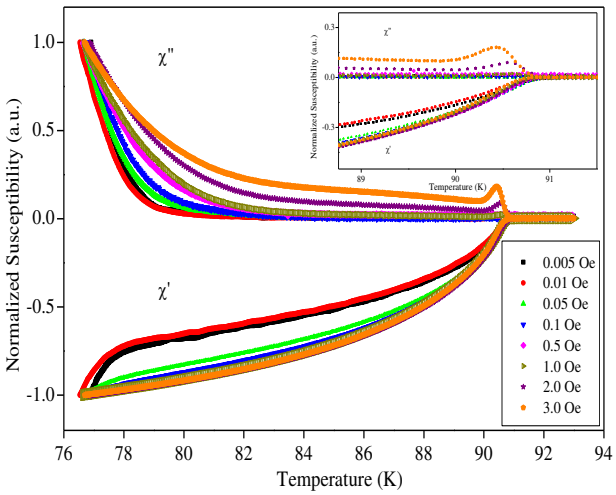

(d)

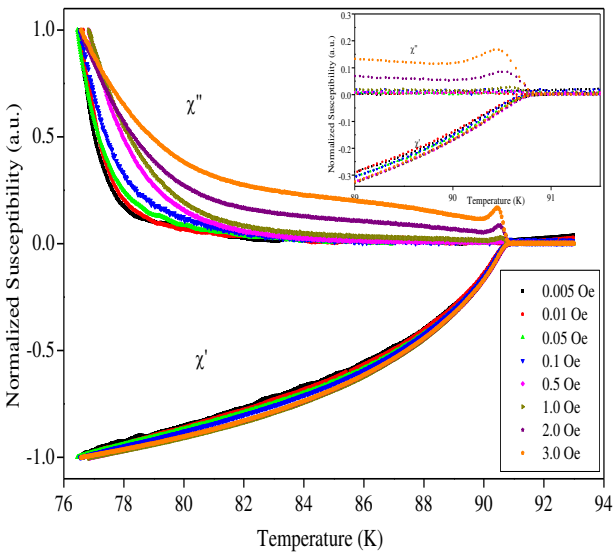

(e)

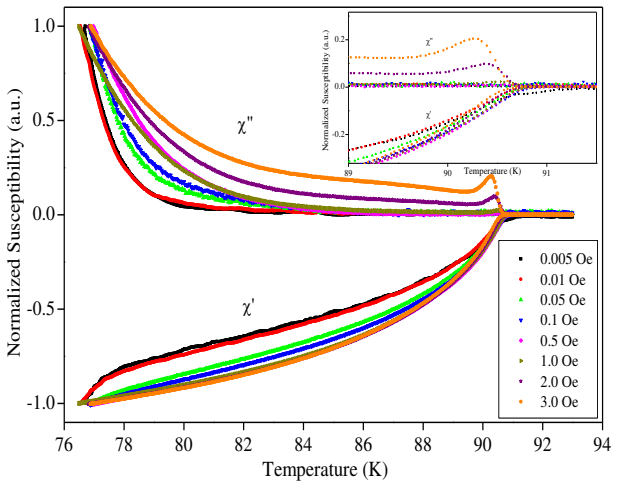

(f)

Figure -7. AC susceptibility of YBCO with addition of Gd_2O_3; (a) = 0.0 wt%, (b) = 0.2 wt%, (c) = 0.4 wt%, (d) = 0.6 wt%, (e) = 0.8 wt% and (f) = 1.0 wt% at frequency 123 Hz and various applied field.

4. CONCLUSIONS

All samples have been successfully prepared by coprecipitation method with the magnetic nanoparticle, Gd_2O_3 was commenced into YBCO bulk through the final sintering procedure. From TG and DTG measurement, the sintering temperature for YBCO 123 was about 900 - 920°C. Above 950°C, the superconducting YBCO phase is damaged due to oxygen loss and melting. In the case of phase formation, the XRD patterns showed that pure sample dominantly single phase and consist of perovskite-like structure Y123 corresponding to orthorhombic *Pmmm* symmetry. However, in the case of the addition of magnetic nanoparticles, the secondary phase showed the existence of semiconducting phase Y_2BaCuO_5 (Y211) which is commonly observed to coexist in YBCO (123) and impurity were observed in all samples. The variation in lattice constants, *a*, *b* and *c* and volume fraction showed that the orthorhombic distortion sensitively depends on the oxygen content and the ionic radius of the RE.This may contributes to the reduction of critical temperature, T_c from 92 K to 88 K. The SEM images showed that the porosity increased and the particle sizes became smaller. From the temperature dependence of ac susceptibility, the inter-granular peaks were only observed in the sample x = 0.2 wt% with the T_p shifted to lower temperature as the applied field increased. In the case of x = 0.4 – 1.0 wt%, the intra-granular peak is clearly able to be seen and height of peak slightly increases. A broad separation between inter- and intra-granular loss peaks indicates that the grains were not well-coupled. Because of ac susceptibility measurement is temperature dependence, this measurement should be done in lower temperature (liquid helium) so that the inter-granular peak is visible and further investigation could be done.

ACKNOWLEDGEMENTS

This work was supported by ERGS Grant (5527047), University Putra Malaysia through the Putra Grant (No. 9440100), Ministry of Education Malaysia (MOE) and University Malaysia Terengganu (UMT). The authors would like also to thank the valuable supports and discussions by all members of Superconductor and Thin Film Laboratory of University Putra Malaysia.

REFERENCES

[1] Cava R.J., Batlogg B., van Dover R. B., Murphy D. W., Sunshine S., Siegrist T., Remeika J. P., Rietman E. A., Zahurak S. and Espinosa G. P. 1987. Bulk superconductivity at 91K in single-phase oxygen-deficient perovskite. Physical Review Letter. 58(16): 1676-1679.

[2] Pathak L. C., Mishra S. K., Bhattacharya D. and Chopra K. L. 1997. A comparative study of YBCO powders prepared by different processes. Journal of Materials Science Letters. 16: 1208-1211.

[3] Manthiram A. and Goodenough J. B. 1987. Synthesis of the high-T_c superconductor $YBa_2Cu_3O_{7-\delta}$ in small particle size. Nature. 329: 701-703.

[4] Kourtakis K., Robbins M. and Gallagher P. K. 1989. A novel synthetic method for the preparation of oxide superconductors: Anionic oxidation-reduction. Journal of Solid State Chemistry. 82: 290-297.

[5] Bhattacharya D., Pathak L. C., Mishra S. K., Sen D. and Chopra K. L. 1990. Pyrophoricsynthesis technique for multicomponent high-temperature superconductors. Applied Physics Letter. 57: 2145.

[6] Sun L. J., Li W., Liu S. f., Mertelj T. and Yao X. 2009. Growth of a high performance SmBCO bulk superconductor with the addition of a $Sm_2Ba_4Cu_2O_9$ phase. Superconductor Science Technology. 22: 125008.

[7] Mellekh A., Zouaoui M., Ben Azzouz F., Annabi M. and Ben Salem M. 2006. Nano-Al_2O_3 particle addition effects on $YBa_2Cu_3O_y$ superconducting properties. Solid State Communications. 140: 318-323.

[8] Jorgensen J. D., Veal B. W., Paulikas A. P., Nowicki G. W., Clausm H. and Kwok W. K. 1990. Structural properties of oxygen-deficient $YBa_2Cu_3O_{7-\delta}$. Physical Review B. 41(4): 1863-1877.

[9] Haugan T., Barnes P. N., Wheeler R., Meisenkothen F. and Sumption M.2004. Addition of nanoparticle

dispersions to enhance flux pinning of the $YBa_2Cu_3O_{7-x}$ superconductor. Nature. 430: 867-870.

[10] Wahid M. H., Zainal Z., Hamadneh I., Tan K. B., Halim S. A., Rosli A. M., Alaghbari E. S., Nazarudin M. F. and Kadri E. F. 2012. Phase formation of $REBa_2Cu_3O_{7-\delta}$ (RE: $Y_{0.5}Gd_{0.5}$, $Y_{0.5}Nd_{0.5}$, $Nd_{0.5}Gd_{0.5}$) superconductors from nanopowders synthesised via co-precipitation. Ceramics International. 38: 1187-1193.

[11] Ochsenkuhn-Petropoulou M., Argyropoulou R., Tarantilis P., Kokkinos E., Ochsenkuhn K. M. and Parissakis G. 2002. Comparison of the oxalate co-precipitation and the solid state reaction methods for the production of high temperature superconducting powders and coatings. Journal of Materials Processing Technology. 127: 122-128.

[12] Giri R., Awana V. P. S., Singh H. K., Tiwari R., S., Srivastava O. N., Anurag Gupta, Kumarawamy H. K. and Kisnan H. 2005. Effect of Ca doping for Y on structural/microstructural and superconducting properties of $YBa_2Cu_3O_{7-\delta}$. Physica C.419: 101-108.

[13] Xu S., Wu X. S., Ma G. B., Wang Z. H. and Gao J. 2008. Effects of Gd_2O_3 addition in $YBa_2Cu_3O_{7-\delta}$ on the critical current density. Journal of Applied Physics. 103: 07C714-07C714-3.

[14] Cava R. J., Battlogg B., Chen C. H., Rietman E. A., Zahurak M. and Werder D. 1987. Oxygen stoichiometry, superconductivity and normal-state properties of $YBa_2Cu_3O_{7-\delta}$. Nature. 329: 423-425.

[15] Tallon J. L., Bernhard C., Shaked H., Hitterman R. L. and Jorgensen J. D. 1995. Generic superconducting phase behavior in high-$T_c$cuprates: T_c variation with hole concentration in $YBa_2Cu_3O_{7-\delta}$ Physical Review B. 51: 12911-12914.

[16] Padam G. K., Raman V., Dhingra I., Tripathi R. B., Rao S. U. M., Suri D. K., Nagpal K. C. and Das B. K. 1991. Synthesis and characterization of Y-Ba-Cu-O and Bi(Pb)-Sr-Ca-Cu-O superconductors from the oxine co-precipitation method. Journal Physics Condensed Matter. 3: 4269-4279.

[17] Sharma D., Kumar R. and Awana V. P. S. 2013. DC and AC Susceptibility study of sol-gel synthesized $Bi_2Sr_2CaCu_2O_{8+\delta}$ superconductor. Ceramics International.*39*: 1143-1152.

[18] Tripodi P., Di Gioacchino D., Celani F., Spallone A. and Shi D. 1997. Frequency dependence of the higher harmonics susceptibilities of hydrogen loaded and unloaded melted YBCO samples. Physica C 282-287: 2329-2330.

[19] Salamati H. and Kameli P. 2004. AC susceptibility study of YBCO thin film and BSCCO bulk superconductors. Journal of Magnetism and Magnetic Materials. 278: 237-243.

[20] Lee C. Y. and Kao Y. H. 1996. Frequency dependence of the intergranular energy-loss peak in AC magnetic susceptibility of high-$T_c$superconductors. Physica C. 256: 183-190.

[21] Çelebi S., Malik A. I. and Halim S. A. 2002. Study of Nd substitution in Bi-(Pb)-Sr-Ca-Cu-O high T_c superconductors. Journal of Alloys and Compounds. 337: 237-242.